Published OnlineFirst August 18, 2011; DOI: 10.1158/0008-5472.CAN-11-1042

Molecular and Cellular Pathobiology

Cancer Research

A Mutation Threshold Distinguishes the Antitumorigenic Effects of the Mitochondrial Gene *MTND1*, an *Oncojanus* Function

Giuseppe Gasparre[1], Ivana Kurelac[1], Mariantonietta Capristo[2], Luisa Iommarini[2], Anna Ghelli[2], Claudio Ceccarelli[7], Giordano Nicoletti[8], Patrizia Nanni[3], Carla De Giovanni[3], Katia Scotlandi[8], Christine M. Betts[4], Valerio Carelli[5], Pier Luigi Lollini[6], Giovanni Romeo[1], Michela Rugolo[2], and Anna Maria Porcelli[2]

Abstract

The oncogenic versus suppressor roles of mitochondrial genes have long been debated. Peculiar features of mitochondrial genetics such as hetero/homoplasmy and mutation threshold are seldom taken into account in this debate. Mitochondrial DNA (mtDNA) mutations generally have been claimed to be protumorigenic, but they are also hallmarks of mostly benign oncocytic tumors wherein they help reduce adaptation to hypoxia by destabilizing hypoxia-inducible factor-1α (HIF1α). To determine the influence of a disassembling mtDNA mutation and its hetero/homoplasmy on tumorigenic and metastatic potential, we injected mice with tumor cells harboring different loads of the gene *MTND1* m.3571insC. Cell cultures obtained from tumor xenografts were then analyzed to correlate energetic competence, apoptosis, α-ketoglutarate (α-KG)/succinate (SA) ratio, and HIF1α stabilization with the mutation load. A threshold level for the antitumorigenic effect of *MTND1* m.3571insC mutation was defined, above which tumor growth and invasiveness were reduced significantly. Notably, HIF1α destabilization and downregulation of HIF1α-dependent genes occurred in cells and tumors lacking complex I (CI), where there was an associated imbalance of α-KG/SA despite the presence of an actual hypoxic environment. These results strongly implicate mtDNA mutations as a cause of oncocytic transformation. Thus, the antitumorigenic and antimetastatic effects of high loads of *MTND1* m.3571insC, following CI disassembly, define a novel threshold-regulated class of cancer genes. We suggest these genes be termed *oncojanus* genes to recognize their ability to contribute either oncogenic or suppressive functions in mitochondrial settings during tumorigenesis. *Cancer Res; 71(19); 6220–9. ©2011 AACR.*

Introduction

Genes encoded by mitochondrial DNA (mtDNA) have long been suspected to be actively involved in tumorigenesis when cells require high amounts of energy to grow and proliferate under few constraints. Although the association between somatic mtDNA mutations and cancer has been widely shown, the mechanistic role played by these mutations is far from being elucidated. The most credited hypothesis is that they may foster tumor progression in various ways such as through effects on regulation of apoptosis, hypoxia-inducible factor-1α (HIF1α) stabilization, and reactive oxygen species (ROS) production and hence metastatic potential (1–4). A question still open in cancer biology concerns the oncogenic versus the oncosuppressor behavior of metabolic genes (5, 6), which incorporate both nuclear- and mtDNA-encoded respiratory complex subunits. Enzymes such as succinate dehydrogenase and fumarate hydratase are actively involved in tumorigenesis, through imbalance of the tricarboxylic acid (TCA) cycle and stabilization of HIF1α (7, 8). Similarly, respiratory complex I (CI) genes may be crucial in regulating cancer cell metabolism, because their function directly impinges on TCA. Alteration of oxidative metabolism resulting from mtDNA mutations may sustain, along with other causes, the triggering of the Warburg Effect that characterizes cancer cells and permits a shift toward glycolysis, hence aiding tumor progression (9, 10). In this context, changes in the metabolic status of cancer cells are closely related to the degree of respiratory chain dysfunction, which, in turn, depends on both mtDNA mutation type (hampering function and/or assembly of complexes) and mutation load.

Reports that describe association of non-neutral mtDNA mutations with all types of cancers do not dwell on the

Authors' Affiliations: [1]Dipartimento di Scienze Ginecologiche, Ostetriche e Pediatriche, Genetica Medica, [2]Dipartimento di Biologia Evoluzionistica Sperimentale, [3]Sezione di Cancerologia, Dipartimento di Patologia Sperimentale, [4]Dipartimento di Patologia Sperimentale, [5]Dipartimento di Scienze Neurologiche, and [6]Dipartimento di Ematologia e Scienze Oncologiche, Università di Bologna; [7]Unità Operativa di Anatomia e Istologia Patologica, Policlinico Universitario S. Orsola-Malpighi; and [8]Laboratorio di Oncologia Sperimentale, Istituti Ortopedici Rizzoli, Bologna, Italy

Note: Supplementary data for this article are available at Cancer Research Online (http://cancerres.aacrjournals.org/).

Corresponding Author: Anna Maria Porcelli, Dipartimento di Biologia Ev. Sp., Università di Bologna, Via Irnerio 42, Bologna, Italy. Phone: 39-051-2091282; Fax: 39-051-242576; E-mail: annamaria.porcelli@unibo.it

doi: 10.1158/0008-5472.CAN-11-1042

©2011 American Association for Cancer Research.

Downloaded from cancerres.aacrjournals.org on September 21, 2021. © 2011 American Association for Cancer Research.

Published OnlineFirst August 18, 2011; DOI: 10.1158/0008-5472.CAN-11-1042

peculiar features of mitochondrial genetics, namely, the concept of homo- versus heteroplasmy, that is, the coexistence of different mtDNA genotypes. Evaluation of the effects of mtDNA mutations must take into account the existence of a threshold above which a pathologic phenotype becomes evident, due to the physiologic polyploidy of the mitochondrial chromosome, which has all too rarely been considered when dissecting the mechanisms underlying the metabolic adaptation of cancer (3). In the vast majority of cases, clearly damaging mtDNA mutations described in tumors are reported as homoplasmic, suggesting that they may determine a pathologic phenotype despite an apparent positive selection (11–19).

A specific subset of tumors, namely oncocytic neoplasias, harbors high loads of damaging mtDNA mutations and yet retains, in most cases, a benign, low-proliferating, noninvasive behavior (12–14, 20–23). A strong association between CI disruption and HIF1α destabilization has been shown through increase of α-ketoglutarate (α-KG)/succinate (SA) ratio, which may be responsible for a higher affinity/activity of the prolyl hydroxylase (PHD) that mediates HIF1α proteasomal degradation. Such metabolic switch was suggested to explain why oncocytic tumors might escape malignancy (23). Thus, certain mtDNA mutations may indeed contribute to reduced tumor growth, depending on their effect on respiratory complex assembly and their heteroplasmy threshold, which, to the best of our knowledge, has never been defined so far.

Here, we show that high loads of a disruptive CI mutation frequently associated with human tumors (11, 12, 14, 15) hamper tumorigenic potential *in vitro* and *in vivo*. Threshold level for antitumorigenic effect of a mtDNA mutation in cancer, leading to oncocytic transformation, was determined, allowing us to define a novel type of tumor-implicated gene, namely the double-edged *oncojanus*.

Materials and Methods

Cell cultures and growth conditions

Human thyroid carcinoma cell line XTC1 was derived from an oncocytic thyroid tumor (24). ZTC1 cells were a heteroplasmic clone obtained by serial dilution of XTC1 (22). Cybrids HXTC1 and HZTC1 were generated from human osteosarcoma 143B.TK cells and previously characterized (23). They will be renamed here as OS-93 and OS-85, respectively, the numbers indicating the percentage of *MTND1* mutation load. A parental control cybrid (CC), previously characterized (23), homoplasmic wild-type for the m.3571insC and belonging to the same mtDNA haplogroup as OS-93 and OS-85, was also used. OSC-83 and OSC-78 were derived from xenografts after *in vivo* injection of OS-85 cells. Cybrid cell lines were grown in Dulbecco's modified Eagle's medium (DMEM), as previously described (23).

All cell lines were authenticated by mtDNA genotyping. Occurrence of the m.3571insC mutation and accurate quantification of heteroplasmy levels as previously described (25) were verified before and after explant as well as before each *in vitro* experiment. To the best of our knowledge, no other cell line is known to harbor such mutation. Moreover, to authenticate cybrid cell lines, the occurrence of the known *TP53* mutation g.13055G>C harbored by the parental 143B.TK cells was verified (Supplementary Fig. S5). Coexistence of the *TP53* mutation along with the m.3571insC unequivocally identified cybrids, whereas thyroid cell lines harbored exclusively the m.3571insC mutation.

Cell viability measurement

Cells (4×10^4) were incubated in glucose-free DMEM supplemented with 5 mmol/L galactose, 5 mmol/L Na-pyruvate, and 10% FBS (DMEM–galactose). Viability was determined by the colorimetric sulforhodamine B assay (26).

CI activity and ATP synthesis

CI assembly and in-gel activity were determined after Blue-Native electrophoresis of isolated mitochondria, as previously described (27). The rate of mitochondrial ATP synthesis driven by CI and complex II (CII) was determined in aliquots of digitonin-permeabilized cells and normalized on citrate synthase activity as previously described (28). Briefly, aliquots of cells (0.1–0.2 mg protein) were incubated with 5 mmol/L malate plus 5 mmol/L pyruvate (CI substrates) or with 10 mmol/L SA (CII substrate) plus 2 μg/mL rotenone. The reaction was started by the addition of 0.2 mmol/L ADP in the presence of luciferine/luciferase, and chemiluminescence was evaluated as a function of time with a luminometer. After the addition of 10 μmol/L oligomycin, the chemiluminescence signal was calibrated with an internal ATP standard.

Soft agar assay

Anchorage-independent cell growth was determined in 0.33% agarose with a 0.5% agarose underlayer. Cell suspensions (1×10^4 to 3×10^4 cells) were plated in semisolid medium. Colonies were counted after 14 days at a magnification of ×40 with an inverted microscope (Nikon Diaphot).

In vivo studies

Cells (3×10^6) were suspended in 0.2 mL sterile PBS and injected s.c. in different strains of immunodeficient mice: 4- to 7-week-old athymic Crl:CD-1-*Foxn1*$^{nu/nu}$ mice (referred to as nude mice, purchased from Charles River) and 23- to 31-week-old Rag2$^{-/-}$;γc$^{-/-}$ on BALB/c background (given by Drs. T. Nomura and M. Ito, Central Institute for Experimental Animals, Kawasaki, Japan, and then bred in our animal facilities under sterile conditions; ref. 29). Experiments were authorized by the Institutional Review Board of the University of Bologna and carried out according to Italian and European guidelines. Individually tagged virgin female mice (5–15 per experimental group) were used. Tumor growth was assessed with a caliper; volume was calculated as $\pi[\sqrt{(a \times b)}]^3/6$, where a = maximal tumor diameter and b = tumor diameter perpendicular to a. Lungs were stained with black India ink and fixed in Fekete's solution to better outline metastases, which were then counted with a dissecting microscope.

Downloaded from cancerres.aacrjournals.org on September 21, 2021. © 2011 American Association for Cancer Research.

Published OnlineFirst August 18, 2011; DOI: 10.1158/0008-5472.CAN-11-1042

Immunohistochemistry

Immunohistochemical (IHC) staining with antibodies against CI MTND6 subunit (Invitrogen) and HIF1α (Upstate Biotech) was carried out as previously reported (13).

α-KG and SA measurements

Cells were incubated in DMEM with and without glutamine for 24 hours. Measurements of metabolites α-KG and SA were carried out essentially as previously described (23).

Western blotting

Total lysates (80 μg) were separated by 10% to 12% SDS-PAGE, and nitrocellulose membranes were incubated with antibody against actin (1:500; Santa Cruz Biotech) and HIF1α (1:1,000; Bethyl Laboratories). Chemiluminescence signals were measured with a molecular imaging apparatus (Kodak).

DNA extraction and DNA laddering analysis

DNA was kit extracted from snap-frozen samples (Sigma-Aldrich), and 2 μL of DNA was loaded onto 1% agarose gel immediately after the extraction. Fragment sizing was determined through comparison with Gene Ruler 1-kb DNA Ladder (Fermentas Inc.). Extractions from 2 distant tumor areas were carried out for large xenografts to account for tissue heterogeneity.

mtDNA sequencing

Whole mtDNA resequencing was carried out with MitoAll (Applied Biosystems) as previously described (14) to verify that xenografts had not accumulated mutations apart from the m.3571insC.

Heteroplasmy evaluation

Mutant load for m.3571insC was determined with fluorescent PCR (F-PCR). according to the previously optimized protocols for mutations in difficult sequence contexts such as in homopolymers (25). To ensure specificity of the mutant load evaluation, each analysis was carried out in quadruplicate and all samples were run in the same reaction plate.

Electron microscopy and morphometric analysis

Xenograft biopsies were immediately collected and processed (14). Sections (1 μm) were stained with 1% toluidine blue for morphology control and electron microscopy area selection. Thin sections were observed with JEM-1011 Transmission Electron Microscope (JEOL Ltd). For each group, 3 xenografts were analyzed, with at least 2 different areas observed for each tumor to rule out intratumor heterogeneity. For morphometric analysis, 95 mitochondria per sample were measured on electron micrographs (magnification: ×15,000) and statistically analyzed with Olympus iTEM Imaging Software.

Pimonidazole staining

Animals were injected intraperitoneally with 60 mg/kg pimonidazole (Hypoxyprobe-1 Plus Kit; HPI) 3 hours before sacrifice. Xenografts were snap frozen and cut in 10-μm slices. Tissues were fixed for 20 minutes with cold acetone, kept for 1 hour in PBS containing 5% FBS, and incubated for 1 hour with fluorescein isothiocyanate-monoclonal antibody 1 (1:10). Fluorescence was visualized with a digital imaging system using an inverted epifluorescence microscope with ×63/1.4 oil objective (Nikon Eclipse Ti-U; Nikon) at 488 nm. Images were captured with a back-illuminated Photometrics Cascade CCD camera system (Roper Scientific) and elaborated with Metamorph Acquisition/Analysis Software (Universal Imaging Corp.).

RNA extraction and real-time PCR analysis

RNA was extracted from snap-frozen tissues with RNeasy Plus Mini Kit (Qiagen), and cDNA was prepared using SuperScript III Reverse Transcriptase (Invitrogen) following manufacturers' instructions. Gene expression levels of glucose transporter-1 (*GLUT-1*), VEGF factor A (*VEGF-A*), and lactate dehydrogenase A (*LDHA*) were measured with real-time PCR, using SYBR Green chemistry and 7500 Fast Real Time System (Applied Biosystems) through absolute quantification. Primer sequences and PCR conditions are available on request.

Statistics

SigmaStat 3.5 software was used for statistical analysis applying Student *t* test unless otherwise indicated.

Results

High loads of the *MTND1* m.3571insC mutation hamper tumor growth

We have previously generated and fully characterized a unique panel of human tumor cell lines harboring the m.3571insC mutation in *MTND1* gene of CI, using 2 different tumor nuclear backgrounds and selecting different levels of heteroplasmy (23). We determined the precise load of mutant mtDNA by F-PCR in all 4 cell lines used, namely, the oncocytic thyroid carcinoma–derived XTC1 (95.5% ± 0.35 mutation load) and ZTC1 (56.7% ± 0.7 mutation load) as well as osteosarcoma-derived cybrids OS-93 (92.8% ± 0.3 mutation load) and OS-85 (85.1% ± 0.8 mutation load). Anchorage-independent growth assay showed that nearly homoplasmic *MTND1* mutant cells (XTC1 and OS-93) formed significantly fewer colonies than heteroplasmic and wild-type cells of the corresponding nuclear background. Interestingly, the heteroplasmic OS-85 cells showed the same *in vitro* growth pattern as the CC (Fig. 1A and B).

To assess whether a high load of the m.3571insC mutation effectively hampered tumor growth *in vivo*, regardless of the nuclear context, we injected all 5 cell lines in 2 different immunodeficient mice models, namely, nude and $Rag2^{-/-};\gamma c^{-/-}$. The growth patterns were coherent in both mice strains, suggesting that the difference in tumorigenic ability observed among cell lines was due to intrinsic properties and not due to the residual immune response of mice. Overall, ZTC1– and OS-85–derived tumors grew significantly larger and faster than their respective high-load mutants XTC1 and OS-93 (Fig. 1C and D; Supplementary Fig. S1). Similarly, CC cells grew in a completely superimposable fashion to OS-85 cells *in vivo*

Downloaded from cancerres.aacrjournals.org on September 21, 2021. © 2011 American Association for Cancer Research.

Published OnlineFirst August 18, 2011; DOI: 10.1158/0008-5472.CAN-11-1042

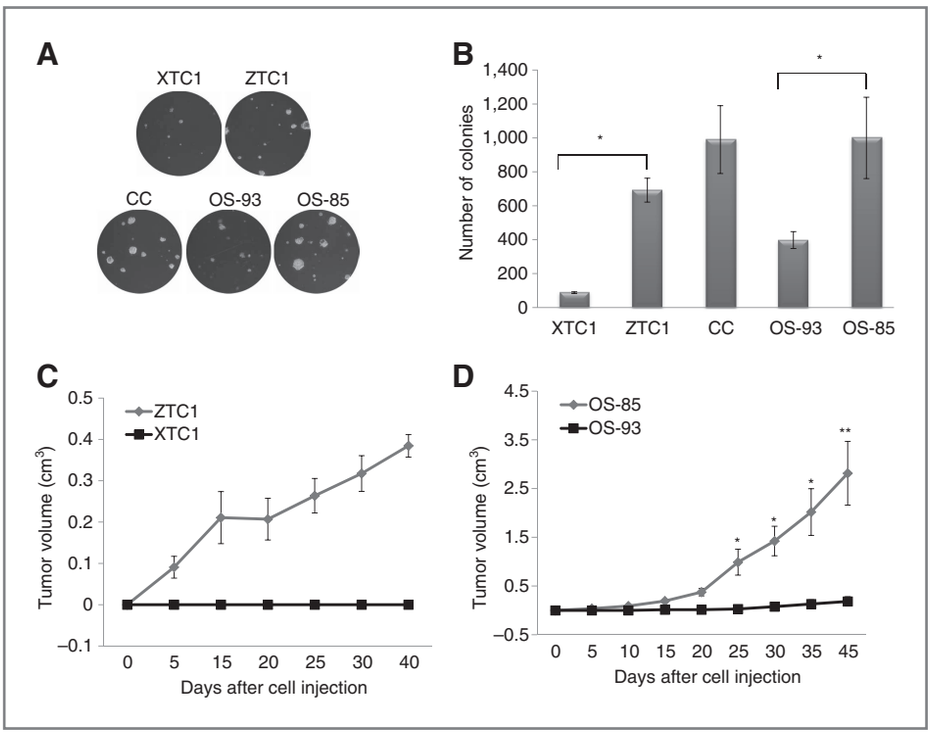

Figure 1. *In vitro* anchorage-independent growth and *in vivo* tumorigenic potential of cell lines. A, representative images of colony growth in soft agar. Magnification, ×40. B, quantification of colonies grown on soft agar plates after 14 days; data are mean ± SD ($n = 4$; *, $P < 0.05$). Tumor growth was generated from thyroid (C) and osteosarcoma (D) cell lines bearing different *MTND1* m.3571insC heteroplasmy levels injected in nude mice. Data are mean ± SEM ($n = 3$, 5 animals for each experiment; *, $P < 0.05$; **, $P < 0.01$).

(not shown), concordantly with previously shown analogous energetic efficiency (23). This finding prompted us to consider that OS-85 cells could be better controls than CC to take further on in subsequent analyses. OS-85 cells also showed a greater metastatic ability than OS-93 cells (Table 1). No other mutations apart from the m.3571insC were detected in xenografts upon resequencing the whole mtDNA. Interestingly, the presence of high loads of mutant mtDNA strongly hampered the growth of the highly aggressive osteosarcoma. On the other hand, the least aggressive was the nearly homoplasmic mutant XTC1 cell line, which failed to grow in any injected animal (Fig. 1C). Most important, high loads of a disruptive CI mutation were sufficient to reduce the tumorigenic potential of at least 2 different types of cancer, osteosarcoma and thyroid carcinoma, regardless of their intrinsic aggressive behavior.

HIF1α destabilization, not apoptosis, contributes to tumor growth reduction

We investigated the possible causes for the observed decrease in tumorigenic potential induced by the high m.3571insC mutation load. Apoptosis has been previously described to be differentially activated in homoplasmic versus heteroplasmic cells (3), yet typical apoptotic DNA laddering and nuclear chromatin condensation were observed exclusively in OS-85–derived tumors, regardless of their hosting mouse strain (Fig. 2A and B), ruling out the role of apoptosis in the reduction of tumorigenic potential. On the basis of the occurrence of a chronic pseudo-normoxic condition in tumors bearing homoplasmic disruptive mtDNA mutations (23), we decided to investigate whether HIF1α destabilization was also induced in xenografts. IHC staining of CI MTND6 subunit was negative in OS-93–derived tumors but positive in most OS-85–derived masses. Correspondingly, HIF1α staining was negative wherever CI suffered from at least partial disassembly (Fig. 2C; ref. 23). Xenografts derived from OS-85 cells showed heterogeneous tumor volumes. Staining with the hypoxic marker pimonidazole (30) revealed that small tumor masses displayed greater hypoxic areas than large ones, indicating that HIF1α stabilization was prevented in CI-deficient tumors despite the low oxygen tension microenvironment *in vivo* (Fig. 2D). Moreover, a significantly lower expression of HIF1α-responding genes, namely, *GLUT-1*, *VEGF-A*, and *LDHA*, was observed in OS-93 xenografts (Fig. 2E), suggesting that HIF1α destabilization had functional consequences on downstream gene expression.

A mutation threshold must be reached to trigger tumor growth inhibition

After detailed analysis of the individual growth curves of OS-85-derived osteosarcoma xenografts, we observed that only a few masses were markedly smaller than the majority (Fig. 3A), which prompted us to quantify precisely the *MTND1* mutation load in all developed tumors. A representative experiment is reported in Fig. 3B. Plotting heteroplasmy levels against tumor volumes in nude mice indicated that only smaller OS-85–derived tumors maintained unaltered the original cell mutation load. On the contrary, all larger tumors underwent a shift toward the wild-type allele (Fig. 3C), suggesting a purifying selection mechanism to overcome the damaging effect of mutations on tumor growth. A threshold for the m.3571insC mutation was hence

Downloaded from cancerres.aacrjournals.org on September 21, 2021. © 2011 American Association for Cancer Research.

Published OnlineFirst August 18, 2011; DOI: 10.1158/0008-5472.CAN-11-1042

Table 1. Tumor and metastasis growth in immunodeficient mice

Cell line	Mice	Incidence (%)		Median number	Range	Significance (Wilcoxon test)
		Tumor	Lung metastases			
OS-85	Nude	15/15 (100)	1/15 (7)	0	0–7	} n.s.
OS-93	Nude	3/10 (30)	1/10 (10)	0	0–1	
OS-85	$Rag2^{-/-};\gamma c^{-/-}$	5/5 (100)	5/5 (100)	>400	237 to >400	} $P < 0.01$
OS-93	$Rag2^{-/-};\gamma c^{-/-}$	5/5 (100)	5/5 (100)	43	4–89	
OSC-78	Nude	5/5 (100)	5/5 (100)	7	1–32	} $P < 0.01$
OSC-83	Nude	5/5 (100)	0/5 (0)	0	0–0	
ZTC1	Nude	10/10 (100)	0/10 (0)	0	0–0	} n.s.
XTC1	Nude	0/10 (0)	0/10 (0)	0	0–0	

Abbreviation: n.s., not significant.

defined between 81% and 83%, above which cancer cells may not sustain mitochondrial energetic impairment. In fact, tumor masses in which the genotype had partly reverted to wild type below 81% presented CI subunit staining (Fig. 2C). A load of more than 83% was therefore sufficient to induce the same phenotype as a load close to homoplasmy, similar to that of OS-93–derived masses. A lower HIF1α protein expression level was observed in smaller OS-85–derived masses above threshold, confirming IHC data (Fig. 3D), and the functional consequences on HIF1α-responding genes expression were comparable with those observed in $Rag2^{-/-};\gamma c^{-/-}$ (Supplementary Fig. S2). Interestingly, no tumor was observed to shift toward the mutant allele, suggesting that random drift may not be the mechanism

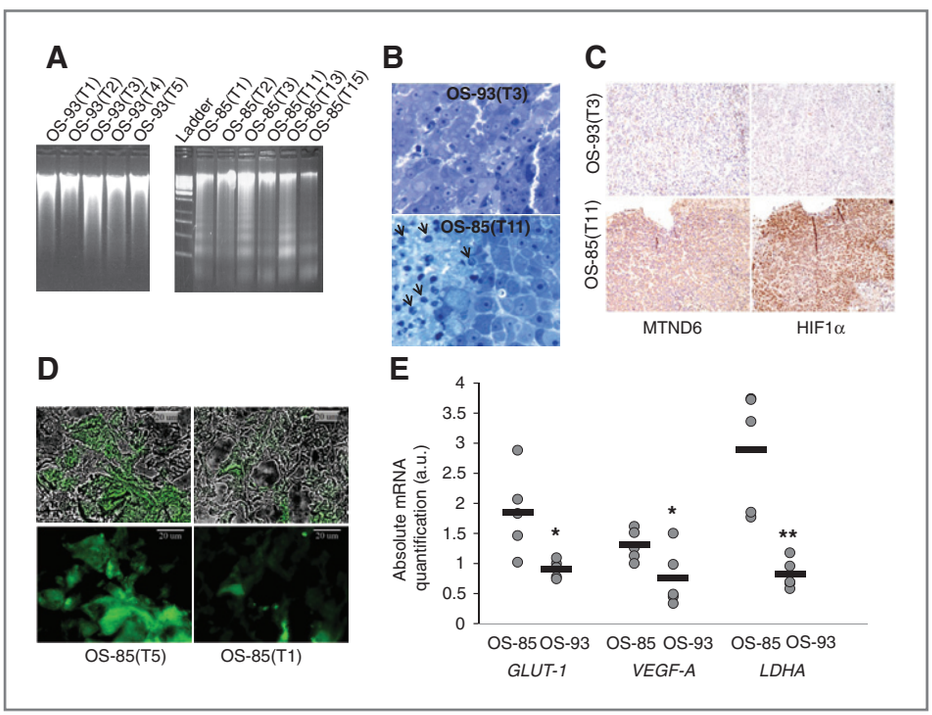

Figure 2. Apoptosis and hypoxia in tumors. A, DNA electrophoresis showing laddering exclusively in OS-85–derived tumors, regardless of hosting mouse strain. Individual tumors generated from OS-85 and OS-93 cells are indicated as OS-85(T*x*) and OS-93(T*x*), where *x* is the number of the hosting mouse. B, nuclear chromatin condensation in high and low mutant load tumors. The black arrows indicate typical rose-shaped nuclei of apoptotic cells. C, representative IHC analysis on dissected tumor masses, using antibodies against MTND6 and HIF1α. Magnification: ×100. D, pimonidazole staining of representative OS-85–derived tumors of different sizes (T1: 3.02 cm^3 and 81% mutation load; T5: 0.31 cm^3 and 84% mutation load). Magnification: ×63. Top, overlay of the images captured at 488 nm (bottom) and in white light. E, gene expression levels of HIF1α-responding genes observed in OS-85 and OS-93 xenografts. Absolute mRNA quantification of *GLUT-1*, *VEGF-A*, and *LDHA* in tumors explanted from $Rag2^{-/-};\gamma c^{-/-}$ mice is reported (*, $P < 0.05$; **, $P < 0.01$). Black bars indicate the average value.

Downloaded from cancerres.aacrjournals.org on September 21, 2021. © 2011 American Association for Cancer Research.

Published OnlineFirst August 18, 2011; DOI: 10.1158/0008-5472.CAN-11-1042

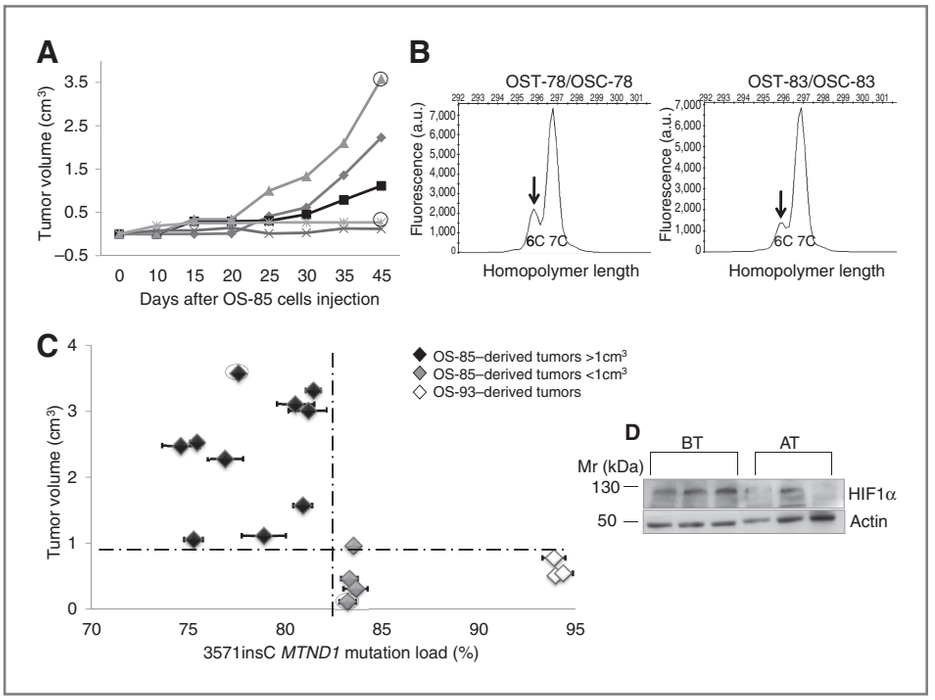

Figure 3. m.3571insC threshold for antitumorigenic effect. A, growth curves of tumors generated after injection with OS-85 cells. One experiment on 5 nude mice representative of 3 independent experiments, for a total of 15 mice, is shown. Circles indicate the 2 tumor masses chosen for analysis reported in B. B, heteroplasmy levels measured by F-PCR. The arrows indicate the wild-type peaks in 2 tumors chosen for further analyses. C, scatter plot showing that the m.3571insC mutation threshold for antitumorigenic effect lies between 81% and 83%. Every point is the mean value of a quadruplicate determination of mutation load ± SD in tumors obtained in nude mice at day 45 after injection. Tumors chosen for further analyses are circled. D, Western blot analysis of HIF1α in OS-85 tumors explanted from representative nude mice. Actin was used as a loading control. AT, above threshold; BT, below threshold.

determining a change in tumor genotype during progression, when non-neutral mutations are involved.

Tumor growth reduction is closely linked to threshold-determined energetic impairment

To assess the functional effects of the mutation threshold on cell phenotype and tumor growth, the smallest and largest tumors were used for further analyses, bearing 83% (OST-83, above threshold) and 78% (OST-78, below threshold) mutation load, respectively, originating from the very same culture batch of OS-85. Cell cultures were generated from xenografts (Fig. 3A) and OSC-83 and OSC-78 cells were obtained (82.8% ± 1.5 and 78.3% ± 1.3 mutation load, respectively, Fig. 3B) carrying identical heteroplasmy levels to those measured in xenografts. Viability of OSC-78 cells after 48 hours of incubation in galactose medium was significantly higher than OSC-83 and than the original OS-85 cells (Fig. 4A). Therefore, only cells bearing a mutation load below the threshold could grow when forced to use oxidative phosphorylation solely for energy production. CI assembly and activity were markedly reduced in OSC-83, whereas no difference in CII–driven ATP synthesis was observed, suggesting no alteration of the remaining oxidative phosphorylation (Fig. 4B). Furthermore, the α-KG/SA ratio was significantly higher in OSC-83 than in OSC-78, both in the presence and absence of glutamine (Fig. 4C), showing that CI disruption influenced the balance of these TCA cycle metabolites and that α-KG production in OSC-83 cells was glutaminolysis independent. Instead of a variation of α-KG levels, such an increase was due to a relevant decrease in SA (Supplementary Table S1). Concordantly, stabilized HIF1α was detected exclusively in OSC-78 (Fig. 4D). When OSC-78 and OSC-83 cells were reinjected in nude mice, OSC-78–derived tumors grew significantly larger than the high-load mutant OSC-83–derived tumors (Fig. 5A), in agreement with the heteroplasmy threshold we have defined (Fig. 5B). Finally, the contribution of ROS overproduction on HIF1α stabilization was ruled out in all clones analyzed. In fact, we failed to observe any significant difference in hydrogen peroxide and anion superoxide levels irrespective of the mutation load (Supplementary Fig. S3A and B).

High loads of m.3571insC trigger oncocytic transformation

The m.3571insC mutation is a hallmark of oncocytic tumors together with similar truncating mutations mainly occurring in homoplasmy (11–15, 21, 23, 31). To verify whether this mutation, when present above threshold, was sufficient to trigger oncocytic transformation, we examined xenografts by electron microscopy. We observed a mitochondria-rich phenotype only in specimens above threshold level (Fig. 6A). A striking resemblance to oncocytic tumors was evident in terms of mitochondria number and swollen

Downloaded from cancerres.aacrjournals.org on September 21, 2021. © 2011 American Association for Cancer Research.

Published OnlineFirst August 18, 2011; DOI: 10.1158/0008-5472.CAN-11-1042

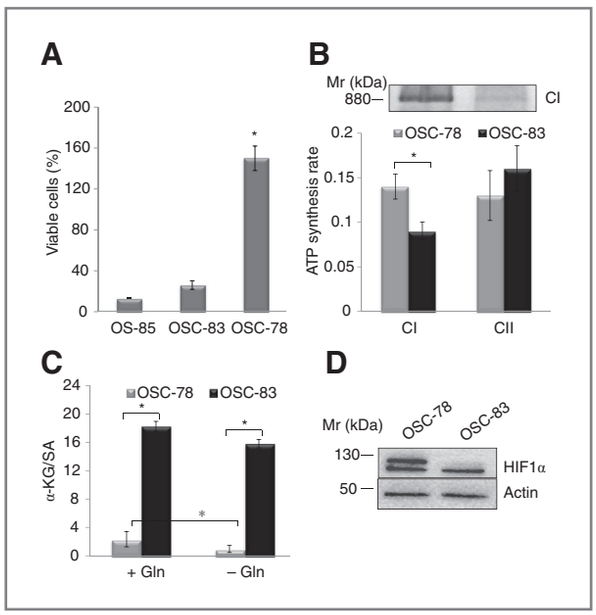

Figure 4. Characterization of OSC-78 and OSC-83 cells. A, viability of cell lines incubated for 48 hours in DMEM–galactose. Data represent mean ± SEM ($n = 5$; *, $P < 0.01$). B, CI in-gel activity. One representative experiment of 3 is shown. Mitochondrial ATP synthesis in digitonin-permeabilized cells driven by pyruvate/malate and SA (CI and CII substrates, respectively) is reported. Rates, normalized for citrate synthase (CS) activity, are mean ± SD ($n = 4$; *, $P < 0.05$). C, the ratio of α-KG and SA levels in the presence (+Gln) and absence (–Gln) of glutamine was calculated by measurements for each metabolite in 3 different experiments (*, $P < 0.05$). D, Western blot analysis of HIF1α in OSC-78 and OSC-83. Actin was used as a loading control. One representative experiment of 3 is shown.

deranged organelle morphology despite the nonepithelial origin of the osteosarcoma xenografts [Fig. 6A (a and c)]. Morphometric analysis showed that both mitochondria area and perimeter of OS-93 tumors were significantly increased compared with those of OS-85 tumors (Fig. 6B and C, respectively; $P < 1E-30$). In fact, mean mitochondria area was approximately (6 ± 2.6)E5 nm^2 in OS-93–derived tumors whereas it was approximately (1.8 ± 1.1)E5 nm^2 in OS-85 xenografts. Concordantly, mean mitochondria perimeter was approximately 3.4 ± 0.8 μm and approximately 2 ± 0.85 μm, respectively, showing that only OS-93 (above threshold) xenografts displayed mitochondria typical of oncocytic tumors.

The hypothesis that the same threshold of disruptive mtDNA mutations we have here defined accompanies oncocytic change in patients was supported by a reanalysis of more than 100 cases from thyroid, pituitary, salivary gland, kidney, and breast oncocytic neoplasms (12–14, 22, 23). In these tumors, the heteroplasmy of the mtDNA mutations was evaluated. Most of the latter were found to affect CI assembly and presented a mutant load of more than 81%, confirming that this was the threshold needed to acquire an oncocytic phenotype (Supplementary Fig. S4).

Discussion

We have shown here that homoplasmy of a truncating mutation in *MTND1* hampers the tumorigenic and metastatic potential of cancer cells *in vivo*. For the first time, a precise threshold for such mutation, sufficient to increase α-KG/SA ratio, induce HIF1α destabilization, and ultimately trigger growth arrest, has been identified.

Our proof for the principle regarding the antitumorigenic effect of mtDNA truncating mutations was obtained with a unique cell model (23), experimentally reinforced through reinjection of highly isogenic clones OSC-78 and OSC-83, carrying a mutation load below and above threshold, respectively. In agreement with previous observations in patients (23), tumor xenografts bearing a mutation above threshold displayed pseudo-normoxia, showing HIF1α destabilization despite being truly hypoxic. HIF1α is considered to be one of the master regulators of the metabolic adaptation needed by cancer cells to progress to malignancy (7, 8, 32). Therefore, this mechanism, tightly linked to the α-KG/SA imbalance as we have shown, may be sufficient to drive the tumor into a "blind alley" due to both respiratory impairment and lack of HIF1α-dependent glycolysis induction (22). Accumulation of NADH and inhibition of α-ketoglutarate dehydrogenase, rather than

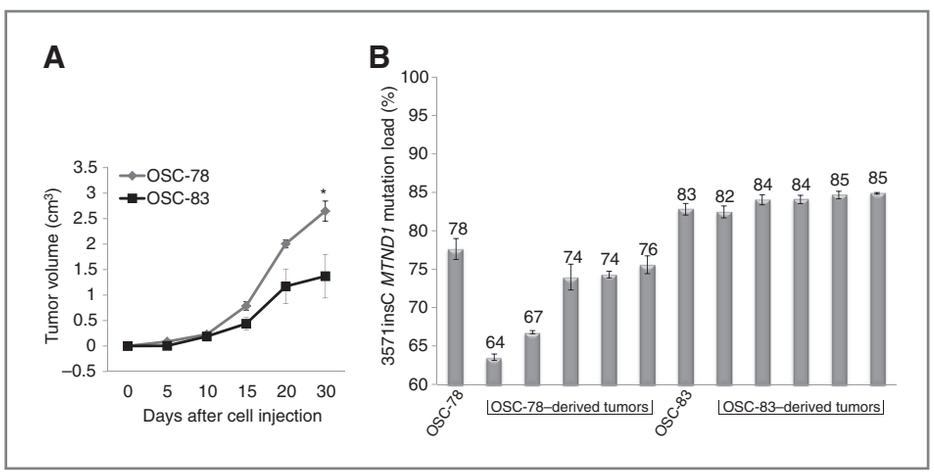

Figure 5. Heteroplasmy levels in OSC-78- and OSC-83–derived tumors. A, tumor growth curves of OSC-78 and OSC-83 injected in nude mice ($n = 2$, 5 animals for each experiment; *, $P < 0.05$). B, mutation loads in tumor masses were evaluated as reported in Materials and Methods. Data are mean ± SD of at least 4 measurements.

Downloaded from cancerres.aacrjournals.org on September 21, 2021. © 2011 American Association for Cancer Research.

Published OnlineFirst August 18, 2011; DOI: 10.1158/0008-5472.CAN-11-1042

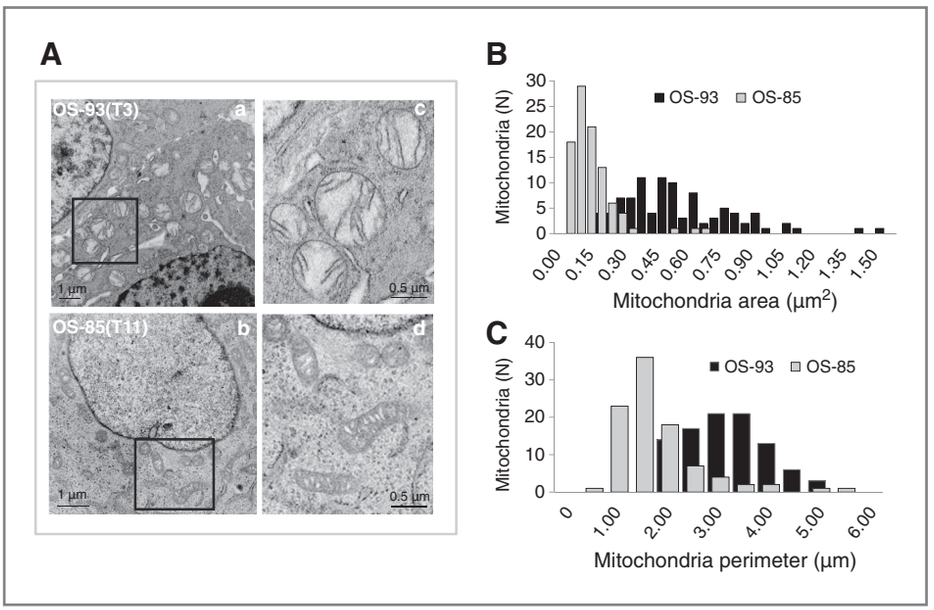

Figure 6. Oncocytic phenotype in osteosarcoma harboring high loads of m.3571insC. A, electron microscopy of representative nude mouse xenografts harboring m.3571insC above [OS-93(T3); a and c] and below [OS-85(T11); b and d] the threshold defined. Numerous, large mitochondria displaying clear matrix and almost total loss of cristae are present in (a) and clearly visible at the higher magnification of the inset (c). A heterogeneous population of mitochondria mostly with darker matrix and normal cristae is shown in (b) and clearly evident at the higher magnification of the inset (d). Morphometric analysis shows the distribution of mitochondria area (B) and perimeter (C) in OS-93 (above threshold) and OS-85 (below threshold) xenografts ($n = 95$).

activation of glutaminolysis (10), may be the most plausible mechanism for α-KG/SA ratio increase as a consequence of CI disassembly. This imbalance may hence either boost the PHD affinity for molecular oxygen or diminish the availability of the main allosteric inhibitor of PHD, that is, SA, determining HIF1α destabilization even during hypoxia (33). In contrast with a previous report by Ishikawa and colleagues (1), who described a higher metastatic potential of cancer cells due to ROS-generating mtDNA mutations, we have ruled out the role of ROS in regulating HIF1α stabilization. This finding is concordant with our previous report (23) and is only apparently in disagreement with that of Ishikawa and colleagues (1), because the type of mtDNA mutation is different in our case. Oncocytic tumors display homoplasmic disassembling CI mutations, such as the m.3571insC here investigated, which may not be a ROS-generating mutation, if one considers that the main ROS production site might be lacking as a whole (23, 34–36). Moreover, the mutant load ought to be considered when analyzing functional effects of mtDNA mutations. The threshold model we propose here implies that, below threshold, CI is present and functioning correctly, in contrast to the case of a missense mutation leading to the coexistence of nonmutant along with mutant, ROS-producing CI.

The most important consideration comes from the strong association between homoplasmic disassembling mtDNA mutations and a mostly benign oncocytic tumor phenotype. Our studies in mice have shown that, upon trespassing the threshold, the mutation is sufficient to trigger oncocytic transformation even in a nonepithelial cancer (Fig. 6A). We have provided evidence that a single mtDNA mutation can generate a specific tumor phenotype, strengthening our hypothesis that mtDNA mutations represent a secondary hit in cancer progression that may determine the oncocytic change subsequently to primary oncogenic transformation (14, 21, 22). Patients with oncocytic tumors rarely present with highly aggressive, metastatic cancers. In the vast majority of cases, these tumors are surgically removed because of hindrance at the site of occurrence, such as in the case of oncocytic pituitary adenoma. In salivary glands, oncocytoma and Warthin tumors are considered benign and even, in some cases, non-neoplastic entities, similarly to oncocytic cells in Hashimoto thyroiditis (37). Kidney oncocytoma is usually considered benign and is only rarely metastatic. Interestingly, the main criterion used to distinguish renal oncocytoma from carcinoma during ultrasound scanning is the absence of vascularization. Our findings provide an explanation for this clinical observation through HIF1α destabilization and, in turn, lack of VEGF pathway activation. In thyroid, criteria for malignancy are independent of oncocytic transformation (37). In our long-standing experience on studying mtDNA sequence variation in all types of oncocytic tumors, the rare metastatic cancers encountered within the large sample set analyzed (>150) were those not harboring mtDNA mutations. Therefore, mtDNA-determined oncocytic transformation seems to be functionally linked to a low tumorigenic and metastatic potential, which highlights the importance of homoplasmy of mtDNA mutations as prognostic markers. Although warranting further investigation, our expression data on HIF1α-responding genes clearly point to a down-modulation of some of the HIF1α pathways as a strong candidate to redirect the tumor fate through the downregulation of neovascularization and glycolytic metabolism. Induction of oncocytic transformation may therefore be envisioned as an approach to reduce tumor growth and abolish aggressive and metastatic potential.

Clinical applications may well arise from the translation of a genetic into a metabolic shift of the α-KG/SA ratio toward α-KG, which supports the use of cell-permeable α-KG derivatives in anticancer therapy (38). Other strategies may impinge on CI disassembly in patients not harboring mtDNA

Downloaded from cancerres.aacrjournals.org on September 21, 2021. © 2011 American Association for Cancer Research.

Published OnlineFirst August 18, 2011; DOI: 10.1158/0008-5472.CAN-11-1042

mutations, degradation of assembly factors, or even modulation of mitochondrial biogenesis to induce both the mutation and its accumulation. In fact, the phenomenon of homoplasmic shift leading to a low-proliferating tumor deserves to be thoroughly understood to be exploited in pathology. In this context, a careful evaluation of the biogenesis and mitophagy pathways leading to mtDNA turnover will likely provide the mechanistic insights underlying the accumulation of non-neutral mtDNA mutations observed in patients.

The findings that tumors grew in mice only when a reversion toward wild type occurred prompt a revision of the Warburg Effect. It seemed that tumors were somehow forced to recover respiration to produce energy and, as our principle showed, stabilize HIF1α. Therefore, certain tumor stages seem to be respiration dependent, most likely until more cell constraints have been removed and neovascularization has commenced together with nutrient influx to sustain a glycolytic shift. A model of waves of gene expression regulation to recover mitochondrial respiration during tumor progression has been recently proposed (10). According to such a model, mitochondria revitalization is a necessary process in the transition from a highly glycolytic to a partial/enhanced oxidative phosphorylation cancer bioenergetic phenotype. Respiration recovery may well not occur in the presence of a homoplasmic mtDNA truncating mutation, strengthening the antitumorigenic effect of CI disassembly.

Interestingly, the threshold we report here for the m.3571insC is analogous to what has been described in MERRF (myoclonic epilepsy and ragged-red fibers) syndrome. In patients with this mitochondrial disease, in fact, the threshold value for the causative m.8344A>G mutation has been described to be 80% (39), which further strengthens the hypothesis that four fifths of mutant mitochondrial genomes in a cell may be sufficient to determine respiratory impairment.

In conclusion, our findings reveal a double-edged functional role for mitochondrial genes, closely correlated to a threshold effect. This property of such genes has allowed us to propose here the definition of *oncojanus*, indicating that, when mutated above a certain load, they determine an energetic impairment that prevents tumor growth.

Disclosure of Potential Conflicts of Interest

No potential conflicts of interest were disclosed.

Grant Support

This work was supported by Associazione Italiana Ricerca sul Cancro—AIRC grants to G. Romeo/M. Rugolo, P.L. Lollini, and K. Scotlandi; by Ministero dell'Istruzione, dell'Università e della Ricerca—MIUR grants PRIN 2008 to A.M. Porcelli and P. Nanni; by FIRB "Futuro in Ricerca" to G. Gasparre; by Pallotti funds to P. Nanni and C.D. Giovanni.

The costs of publication of this article were defrayed in part by the payment of page charges. This article must therefore be hereby marked *advertisement* in accordance with 18 U.S.C. Section 1734 solely to indicate this fact.

Received March 29, 2011; revised July 8, 2011; accepted July 24, 2011; published OnlineFirst August 18, 2011.

References

1. Ishikawa K, Takenaga K, Akimoto M, Koshikawa N, Yamaguchi A, Imanishi H, et al. ROS-generating mitochondrial DNA mutations can regulate tumor cell metastasis. Science 2008;320:661–4.
2. Shidara Y, Yamagata K, Kanamori T, Nakano K, Kwong JQ, Manfredi G, et al. Positive contribution of pathogenic mutations in the mitochondrial genome to the promotion of cancer by prevention from apoptosis. Cancer Res 2005;65:1655–63.
3. Park JS, Sharma LK, Li H, Xiang R, Holstein D, Wu J, et al. A heteroplasmic, not homoplasmic, mitochondrial DNA mutation promotes tumorigenesis via alteration in reactive oxygen species generation and apoptosis. Hum Mol Genet 2009;18:1578–89.
4. Petros JA, Baumann AK, Ruiz-Pesini E, Amin MB, Sun CQ, Hall J, et al. mtDNA mutations increase tumorigenicity in prostate cancer. Proc Natl Acad Sci U S A 2005;102:719–24.
5. Thompson CB. Metabolic enzymes as oncogenes or tumor suppressors. N Engl J Med 2009;360:813–5.
6. Gottlieb E, Tomlinson IP. Mitochondrial tumour suppressors: a genetic and biochemical update. Nat Rev Cancer 2005;5:857–66.
7. Pollard PJ, Briere JJ, Alam NA, Barwell J, Barclay E, Wortham NC, et al. Accumulation of Krebs cycle intermediates and over-expression of HIF1alpha in tumours which result from germline FH and SDH mutations. Hum Mol Genet 2005;14:2231–9.
8. Selak MA, Armour SM, MacKenzie ED, Boulahbel H, Watson DG, Mansfield KD, et al. Succinate links TCA cycle dysfunction to oncogenesis by inhibiting HIF-alpha prolyl hydroxylase. Cancer Cell 2005;7:77–85.
9. Chen Z, Lu W, Garcia-Prieto C, Huang P. The Warburg effect and its cancer therapeutic implications. J Bioenerg Biomembr 2007;39:267–74.
10. Smolkova K, Plecita-Hlavata L, Bellance N, Benard G, Rossignol R, Jezek P. Waves of gene regulation suppress and then restore oxidative phosphorylation in cancer cells. Int J Biochem Cell Biol 2011;43:950–68.
11. Costa-Guda J, Tokura T, Roth SI, Arnold A. Mitochondrial DNA mutations in oxyphilic and chief cell parathyroid adenomas. BMC Endocr Disord 2007;7:8.
12. Gasparre G, Hervouet E, de LE, Demont J, Pennisi LF, Colombel M, et al. Clonal expansion of mutated mitochondrial DNA is associated with tumor formation and complex I deficiency in the benign renal oncocytoma. Hum Mol Genet 2008;17:986–95.
13. Gasparre G, Iommarini L, Porcelli AM, Lang M, Ferri GG, Kurelac I, et al. An inherited mitochondrial DNA disruptive mutation shifts to homoplasmy in oncocytic tumor cells. Hum Mutat 2009;30:391–6.
14. Gasparre G, Porcelli AM, Bonora E, Pennisi LF, Toller M, Iommarini L, et al. Disruptive mitochondrial DNA mutations in complex I subunits are markers of oncocytic phenotype in thyroid tumors. Proc Natl Acad Sci U S A 2007;104:9001–6.
15. Mayr JA, Meierhofer D, Zimmermann F, Feichtinger R, Kogler C, Ratschek M, et al. Loss of complex I due to mitochondrial DNA mutations in renal oncocytoma. Clin Cancer Res 2008;14:2270–5.
16. Maximo V, Soares P, Lima J, Cameselle-Teijeiro J, Sobrinho-Simoes M. Mitochondrial DNA somatic mutations (point mutations and large deletions) and mitochondrial DNA variants in human thyroid pathology: a study with emphasis on Hurthle cell tumors. Am J Pathol 2002;160:1857–65.
17. Habano W, Sugai T, Yoshida T, Nakamura S. Mitochondrial gene mutation, but not large-scale deletion, is a feature of colorectal carcinomas with mitochondrial microsatellite instability. Int J Cancer 1999;83:625–9.
18. Jeronimo C, Nomoto S, Caballero OL, Usadel H, Henrique R, Varzim G, et al. Mitochondrial mutations in early stage prostate cancer and bodily fluids. Oncogene 2001;20:5195–8.
19. Polyak K, Li Y, Zhu H, Lengauer C, Willson JK, Markowitz SD, et al. Somatic mutations of the mitochondrial genome in human colorectal tumours. Nat Genet 1998;20:291–3.

Downloaded from cancerres.aacrjournals.org on September 21, 2021. © 2011 American Association for Cancer Research.

Published OnlineFirst August 18, 2011; DOI: 10.1158/0008-5472.CAN-11-1042

20. Bonora E, Porcelli AM, Gasparre G, Biondi A, Ghelli A, Carelli V, et al. Defective oxidative phosphorylation in thyroid oncocytic carcinoma is associated with pathogenic mitochondrial DNA mutations affecting complexes I and III. Cancer Res 2006;66:6087–96.
21. Gasparre G, Bonora E, Tallini G, Romeo G. Molecular features of thyroid oncocytic tumors. Mol Cell Endocrinol 2010;321:67–76.
22. Gasparre G, Romeo G, Rugolo M, Porcelli AM. Learning from oncocytic tumors: why choose inefficient mitochondria? Biochim Biophys Acta 2011;1807:633–42.
23. Porcelli AM, Ghelli A, Ceccarelli C, Lang M, Cenacchi G, Capristo M, et al. The genetic and metabolic signature of oncocytic transformation implicates HIF1alpha destabilization. Hum Mol Genet 2010;19:1019–32.
24. Zielke A, Tezelman S, Jossart GH, Wong M, Siperstein AE, Duh QY, et al. Establishment of a highly differentiated thyroid cancer cell line of Hurthle cell origin. Thyroid 1998;8:475–83.
25. Kurelac I, Lang M, Zuntini R, Calabrese C, Simone D, Vicario S, et al. Searching for a needle in the haystack: comparing six methods to evaluate heteroplasmy in difficult sequence context. Biotech Adv 2010 Jun 13. [Epub ahead of print].
26. Porcelli AM, Ghelli A, Iommarini L, Mariani E, Hoque M, Zanna C, et al. The antioxidant function of Bcl-2 preserves cytoskeletal stability of cells with defective respiratory complex I. Cell Mol Life Sci 2008;65:2943–51.
27. Porcelli AM, Angelin A, Ghelli A, Mariani E, Martinuzzi A, Carelli V, et al. Respiratory complex I dysfunction due to mitochondrial DNA mutations shifts the voltage threshold for opening of the permeability transition pore toward resting levels. J Biol Chem 2009;284:2045–52.
28. Ghelli A, Porcelli AM, Zanna C, Vidoni S, Mattioli S, Barbieri A, et al. The background of mitochondrial DNA haplogroup J increases the sensitivity of Leber's hereditary optic neuropathy cells to 2,5-hexanedione toxicity. PLoS One 2009;4:e7922.
29. Nanni P, Nicoletti G, Landuzzi L, Croci S, Murgo A, Palladini A, et al. High metastatic efficiency of human sarcoma cells in Rag2/gammac double knockout mice provides a powerful test system for antimetastatic targeted therapy. Eur J Cancer 2010;46:659–68.
30. Chen Y, Cairns R, Papandreou I, Koong A, Denko NC. Oxygen consumption can regulate the growth of tumors, a new perspective on the Warburg effect. PLoS One 2009;4:e7033.
31. Zimmermann FA, Mayr JA, Neureiter D, Feichtinger R, Alinger B, Jones ND, et al. Lack of complex I is associated with oncocytic thyroid tumours. Br J Cancer 2009;100:1434–7.
32. Maxwell PH, Pugh CW, Ratcliffe PJ. Activation of the HIF pathway in cancer. Curr Opin Genet Dev 2001;11:293–9.
33. Bruick RK. Oxygen sensing in the hypoxic response pathway: regulation of the hypoxia-inducible transcription factor. Genes Dev 2003;17:2614–23.
34. Tuppen HA, Hogan VE, He L, Blakely EL, Worgan L, Al-Dosary M, et al. The p.M292T NDUFS2 mutation causes complex I-deficient Leigh syndrome in multiple families. Brain 2010;133:2952–63.
35. Morán M, Rivera H, Sánchez-Aragó M, Blázquez A, Merinero B, Ugalde C, et al. Mitochondrial bioenergetics and dynamics interplay in complex I-deficient fibroblasts. Biochim Biophys Acta 2010;1802:443–53.
36. Koopman WJ, Verkaart S, Visch HJ, van Emst-de Vries S, Nijtmans LG, Smeitink JA, et al. Human NADH:ubiquinone oxidoreductase deficiency: radical changes in mitochondrial morphology? Am J Physiol Cell Physiol 2007;293:C22–9.
37. Tallini G. Oncocytic tumours. Virchows Arch 1998;433:5–12.
38. MacKenzie ED, Selak MA, Tennant DA, Payne LJ, Crosby S, Frederiksen CM, et al. Cell-permeating alpha-ketoglutarate derivatives alleviate pseudohypoxia in succinate dehydrogenase-deficient cells. Mol Cell Biol 2007;27:3282–9.
39. Boulet L, Karpati G, Shoubridge EA. Distribution and threshold expression of the tRNA(Lys) mutation in skeletal muscle of patients with myoclonic epilepsy and ragged-red fibers (MERRF). Am J Hum Genet 1992;51:1187–200.

Downloaded from cancerres.aacrjournals.org on September 21, 2021. © 2011 American Association for Cancer Research.

Published OnlineFirst August 18, 2011; DOI: 10.1158/0008-5472.CAN-11-1042

Cancer Research
The Journal of Cancer Research (1916–1930) | The American Journal of Cancer (1931–1940)

AACR American Association for Cancer Research

A Mutation Threshold Distinguishes the Antitumorigenic Effects of the Mitochondrial Gene *MTND1*, an *Oncojanus* Function

Giuseppe Gasparre, Ivana Kurelac, Mariantonietta Capristo, et al.

Cancer Res 2011;71:6220-6229. Published OnlineFirst August 18, 2011.

Updated version	Access the most recent version of this article at: doi:10.1158/0008-5472.CAN-11-1042
Supplementary Material	Access the most recent supplemental material at: http://cancerres.aacrjournals.org/content/suppl/2011/08/18/0008-5472.CAN-11-1042.DC1

Cited articles	This article cites 38 articles, 9 of which you can access for free at: http://cancerres.aacrjournals.org/content/71/19/6220.full#ref-list-1
Citing articles	This article has been cited by 7 HighWire-hosted articles. Access the articles at: http://cancerres.aacrjournals.org/content/71/19/6220.full#related-urls

E-mail alerts	Sign up to receive free email-alerts related to this article or journal.
Reprints and Subscriptions	To order reprints of this article or to subscribe to the journal, contact the AACR Publications Department at pubs@aacr.org.
Permissions	To request permission to re-use all or part of this article, use this link http://cancerres.aacrjournals.org/content/71/19/6220. Click on "Request Permissions" which will take you to the Copyright Clearance Center's (CCC) Rightslink site.

Downloaded from cancerres.aacrjournals.org on September 21, 2021. © 2011 American Association for Cancer Research.